

# Non-uniform ENO Scheme for Simulation of Supersonic Flows

Yekaterina Moisseyeva, Altynshash Naimanova and Asel Beketaeva

Al-Farabi Kazakh National University, Al-Farabi 71, Almaty, 050040, Kazakhstan  
k.moisseyeva@gmail.com, alt\_naimanova@yahoo.com, azimaras@mail.ru

**Abstract.** The third order finite-difference shock-capturing essentially non-oscillatory (ENO) scheme for a non-uniform grid has been developed. The design of the ENO scheme is based on the methodology for uniform grids. The efficiency of the developed algorithm is demonstrated by the numerical experiments on the simulation of the three-dimensional turbulent steady flowfield generated by the transverse hydrogen injection into the supersonic air cross-flow. The analysis of the different variations of the limiter functions for the developed algorithm is provided to define the optimal function producing the smallest spread of the solution. The effect of the limiter choice on the mixing layer dynamics is studied for the non-uniform grid. The numerical experiments revealed that the nonoptimal choice of limiter can result in the overgrowth of the mixing layer, that is important for the numerical modeling of the combustion.

**Keywords:** ENO scheme, non-uniform grid, slope limiters, supersonic flow, transverse injection, multispecies gas

## 1 Introduction

The study of the transverse injection into a supersonic flow is an important issue in the modeling of the supersonic combustion in scramjets. The mixing flowfield is very complex, the Fig. 1 shows the general structure of the supersonic freestream with the transverse injected jet [1,2]. A three-dimensional bow shock forms ahead the injection and interacts with the boundary layer, producing the separation shock. The separated region results in a smaller weak shock, and these three shocks create the lambda shock structure. The underexpanded jet jet emerges from the orifice and expands to the freestream pressure at the jet boundary, the barrel shock occurs. Acceleration of the jet flow continues until a normal shock (Mach disk) forms, behind which the flow becomes subsonic and accelerates then downstream to the mainflow velocity value. Further downstream the jet boundary takes the form of a pair of the counter rotating vortices. The horseshoe-vortex wraps around the jet and forms the wake vortices. Also there is another recirculation zone downstream of the jet due to the rarefaction behind the jet.

To capture these complex structures, in the regions of the large gradients (in the boundary layer, near the wall and on the jet exit) condensation of the grid is introduced and schemes of the high order of accuracy are used. At the present, TVD (Total Variation Diminishing), ENO (essentially non-oscillatory) and WENO (weighted ENO) schemes are successful tools for numerical simulations of supersonic flows. Traditionally these schemes have been derived for a uniform grid with a coordinate system transformation [3,4,5]. Recently, a number of authors [6,7] have investigated applications of TVD schemes to non-uniform grids and analyzed the slope limiters on non-uniform grids.

The objective of the present paper is development of the third order finite-difference shock-capturing ENO scheme for a non-uniform grid. The design of the ENO scheme is based on the methodology for uniform grids proposed by the authors in [8]. Here, the Newton interpolant of the third order degree was adapted for the non-uniform grid to construct the essentially non-oscillatory piecewise polynomial. The efficiency of the developed algorithm is demonstrated by the numerical simulation of the three-dimensional turbulent steady flowfield generated by

the transverse hydrogen injection into the supersonic air cross-flow by solving the Reynolds-averaged Navier-Stokes equations closed by the  $k-\omega$  turbulent model. Additionally, the effective adiabatic parameter of the gas mixture is introduced. It allows one to calculate the derivatives of the pressure with respect to independent variables for determining the Jacobian matrices, and thus to construct an efficient implicit algorithm of the solution. The analysis of the effect of the modified limiter choice on the solution is provided for the numerical simulation of the three-dimensional supersonic air flow with the perpendicular injected hydrogen.

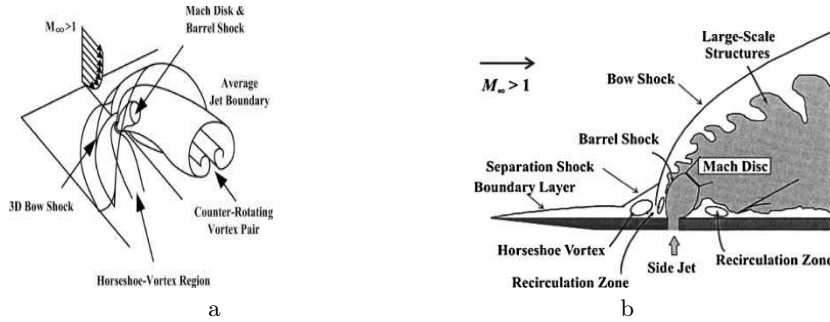


Fig. 1. Schematic diagram of the flowfield [1] (a), in the symmetry section  $xz$  [2] (b)

## 1.1 Governing Equations

Basic equations for the problem are the system of the three-dimensional Reynolds averaged Navier-Stokes equations for the compressible turbulent multispecies gas in the Cartesian coordinate system written in the conservative form as

$$\frac{\partial \mathbf{U}}{\partial t} + \frac{\partial (\mathbf{E} - \mathbf{E}_v)}{\partial x} + \frac{\partial (\mathbf{F} - \mathbf{F}_v)}{\partial y} + \frac{\partial (\mathbf{G} - \mathbf{G}_v)}{\partial z} = 0. \quad (1)$$

Vectors  $\mathbf{U}$ ,  $\mathbf{E}$ ,  $\mathbf{F}$ ,  $\mathbf{G}$  are defined by

$$\begin{aligned} \mathbf{U} &= (\rho, \rho u, \rho v, \rho w, E_t, \rho Y_k)^T, \\ \mathbf{E} &= (\rho u, \rho u^2 + p, \rho uv, \rho uw, (E_t + p)u, \rho u Y_k)^T, \\ \mathbf{F} &= (\rho v, \rho uv, \rho v^2 + p, \rho vw, (E_t + p)v, \rho v Y_k)^T, \\ \mathbf{G} &= (\rho w, \rho uw, \rho vw, \rho w^2 + p, (E_t + p)w, \rho w Y_k)^T, \end{aligned}$$

and vectors  $\mathbf{E}_v$ ,  $\mathbf{F}_v$ ,  $\mathbf{G}_v$  are associated with viscous stress

$$\begin{aligned} \mathbf{E}_v &= (0, \tau_{xx}, \tau_{xy}, \tau_{xz}, u\tau_{xx} + v\tau_{xy} + w\tau_{xz} - q_x, J_{kx})^T, \\ \mathbf{F}_v &= (0, \tau_{xy}, \tau_{yy}, \tau_{yz}, u\tau_{xy} + v\tau_{yy} + w\tau_{yz} - q_y, J_{ky})^T, \\ \mathbf{G}_v &= (0, \tau_{xz}, \tau_{yz}, \tau_{zz}, u\tau_{xz} + v\tau_{yz} + w\tau_{zz} - q_z, J_{kz})^T. \end{aligned}$$

The components of the viscous stress tensor are

$$\begin{aligned} \tau_{xx} &= \frac{2\mu}{3Re} (2u_x - v_y - w_z), \quad \tau_{yy} = \frac{2\mu}{3Re} (2v_y - u_x - w_z), \\ \tau_{zz} &= \frac{2\mu}{3Re} (2w_z - u_x - v_y), \quad \tau_{xy} = \tau_{yx} = \frac{\mu}{Re} (u_y + v_x), \\ \tau_{xz} &= \tau_{zx} = \frac{\mu}{Re} (u_z + w_x), \quad \tau_{yz} = \tau_{zy} = \frac{\mu}{Re} (v_z + w_y). \end{aligned}$$

The heat flux is defined by

$$\begin{aligned} q_x &= \frac{\mu}{PrRe} \frac{\partial T}{\partial x} + \frac{1}{\gamma_\infty M_\infty^2} \sum_{k=1}^N h_k J_{xk} , \\ q_y &= \frac{\mu}{PrRe} \frac{\partial T}{\partial y} + \frac{1}{\gamma_\infty M_\infty^2} \sum_{k=1}^N h_k J_{yk} , \\ q_z &= \frac{\mu}{PrRe} \frac{\partial T}{\partial z} + \frac{1}{\gamma_\infty M_\infty^2} \sum_{k=1}^N h_k J_{zk} , \end{aligned}$$

and the diffusion flux is determined by

$$J_{kx} = -\frac{\mu}{ScRe} \frac{\partial Y_k}{\partial x} , J_{ky} = -\frac{\mu}{ScRe} \frac{\partial Y_k}{\partial y} , J_{kz} = -\frac{\mu}{ScRe} \frac{\partial Y_k}{\partial z} .$$

The pressure and the total energy are

$$p = \frac{\rho T}{\gamma_\infty M_\infty^2} \sum_{k=1}^N \frac{Y_k}{W_k} , E_t = \frac{\rho}{\gamma_\infty M_\infty^2} \sum_{k=1}^N Y_k h_k - p + \frac{1}{2} \rho (u^2 + v^2 + w^2) ,$$

The specific enthalpy and the specific heat at constant pressure of the  $k$ th species are

$$h_k = h_k^0 + \int_{T_0}^T c_{pk} dT , c_{pk} = C_{pk} \left( \sum_{k=1}^N \frac{Y_k}{W_k} \right) ,$$

where the molar specific heat is written in the polynomial form as

$$C_{pk} = \sum_{i=1}^5 \bar{a}_{ki} T^{i-1} ,$$

the coefficients  $\bar{a}_{ki}$  are taken from the thermodynamic tables JANAF [9].

The viscosity coefficient is defined as a sum of the laminar and turbulent viscosity coefficients:  $\mu = \mu_l + \mu_t$ , where  $\mu_l$  is determined by Wilke formula, and  $\mu_t$  is determined by  $k - \omega$  turbulent model [10].

In the system (1)  $u, v, w, \rho, T$  represent the components of the velocity vector, the density and the temperature, respectively.  $Y_k$  and  $W_k$  are the mass fraction and the molecular weight of the  $k$ th species, where  $Y_1$  stands for the mass fraction of  $H_2$ ,  $Y_2$  for the mass fraction of  $O_2$ ,  $Y_3$  for the mass fraction of  $N_2$ .  $\gamma$  is the adiabatic parameter,  $M$  is the Mach number. Index 0 indicates jet parameters and index  $\infty$  indicates parameters of the main flow.

The system (1) is written in a nondimensional form. Constitutive parameters are parameters of the main flow at the inlet ( $u_\infty, \rho_\infty, T_\infty$ ). The injector diameter  $d$  is chosen as the characteristic length.

## 1.2 Boundary Conditions

On the flow field entrance, the parameters of the free stream are given

$$\begin{aligned} p &= p_\infty , T = T_\infty , u = M_\infty \sqrt{\frac{\gamma_\infty R_0 T_\infty}{W_\infty}} , v = w = 0 , Y_k = Y_{k\infty} , W_k = W_{k\infty} , \\ x &= 0 , 0 \leq y \leq H_y , 0 \leq z \leq H_z . \end{aligned}$$

Also boundary layer is given near the wall, the longitudinal velocity component is approximated by the 1/7th power law.

On the injector, the parameters of the jet are given

$$p = np_\infty, \quad T = T_0, \quad u = v = 0, \quad w = M_0 \sqrt{\frac{\gamma_0 R_0 T_0}{W_0}}, \quad Y_k = Y_{k0}, \quad W_k = W_{k0},$$

$$z = 0, \quad |x^2 + y^2| \leq R,$$

where  $n = p_0/p_\infty$  is the pressure ratio.

The non-reflecting boundary conditions are adopted on the flow field exit [11]. The adiabatic no-slip boundary condition on the wall and the symmetry boundary condition on the symmetry faces are specified. Here  $H_x$ ,  $H_y$  and  $H_z$  are the length, width and height of the computational domain, respectively.  $R$  is the injector radius.

## 2 Method of Solution

The problem is solved by the implicit method. The methodology is similar to that on a uniform grid and can be found in [8,12]. Numerical solution is performed in two steps. At the first step the thermodynamic parameters and at the second step the mass fractions are resolved. The conservation equations are discretized using a first-order forward difference operator for the time derivative. The upwind differences of the first order of accuracy have been used for the approximation of the first derivatives, and the central differences of the first order of accuracy have been used for the second derivatives. For the approximation of the convective terms, the ENO scheme of the third order is applied, which will be described below. The obtaining system of equations is solved by the factorization using the matrix sweep method for the vector of the thermodynamic parameters and the tridiagonal inversion for the vector of the mass fractions.

**Finite Difference ENO Scheme on Non-Uniform Grid.** For numerical solution of (1), the ENO scheme of the third order is applied for the inviscid convective fluxes, where the Newton interpolant of the third order degree was adapted for the non-uniform grid to construct the essentially non-oscillatory piecewise polynomial. After that, the reconstruction procedure via primitive function is applied. In accordance with the principle of the ENO scheme, the inviscid convective fluxes are presented as

$$\mathbf{E}^m = \mathbf{E}^{n+1} + (\mathbf{E}_x + \mathbf{D}_x)^n. \quad (2)$$

In (2),  $\mathbf{E}^m$  is the modified flux at the node point  $(i, j, k)$ , which consists of the original convective vector  $\mathbf{E}$  and additional terms of the high order of accuracy  $\mathbf{E}_x$ ,  $\mathbf{D}_x$ :

$$\mathbf{E}_{x,i}^\pm = \pm \text{limiter1}(\bar{\mathbf{E}}_{x,i-1/2}, \bar{\mathbf{E}}_{x,i+1/2}), \quad (3)$$

$$\mathbf{D}_{x,i}^+ = \begin{cases} \text{limiter2}(d_i \bar{\mathbf{D}}_{x,i-1/2}^+, d_{i+1} \bar{\mathbf{D}}_{x,i+1/2}^+), & \text{if } \left| \Delta_- \left( \frac{\Delta_- \mathbf{U}}{s_i} \right) \right| \leq \left| \Delta_+ \left( \frac{\Delta_- \mathbf{U}}{s_i} \right) \right| \\ \text{limiter2}(d_{i+1} \hat{\mathbf{D}}_{x,i+1/2}^+, d_{i+2} \hat{\mathbf{D}}_{x,i+3/2}^+), & \text{if } \left| \Delta_- \left( \frac{\Delta_- \mathbf{U}}{s_i} \right) \right| > \left| \Delta_+ \left( \frac{\Delta_- \mathbf{U}}{s_i} \right) \right| \end{cases}$$

$$\mathbf{D}_{x,i}^- = \begin{cases} \text{limiter2}(d_i \hat{\mathbf{D}}_{x,i-3/2}^-, d_{i+1} \hat{\mathbf{D}}_{x,i-1/2}^-), & \text{if } \left| \Delta_- \left( \frac{\Delta_+ \mathbf{U}}{s_{i+1}} \right) \right| \leq \left| \Delta_+ \left( \frac{\Delta_+ \mathbf{U}}{s_{i+1}} \right) \right| \\ \text{limiter2}(d_{i+1} \bar{\mathbf{D}}_{x,i-1/2}^-, d_{i+2} \bar{\mathbf{D}}_{x,i+1/2}^-), & \text{if } \left| \Delta_- \left( \frac{\Delta_+ \mathbf{U}}{s_{i+1}} \right) \right| > \left| \Delta_+ \left( \frac{\Delta_+ \mathbf{U}}{s_{i+1}} \right) \right| \end{cases}$$

where

$$\begin{aligned}\bar{E}_{x,i-1/2} &= \bar{h}_i \left( I - \frac{\Delta t}{\bar{h}_i} |A_{i-1/2}| \right) \frac{\Delta_- \mathbf{E}_i}{s_i}, \\ \bar{E}_{x,i+1/2} &= \bar{h}_i \left( I - \frac{\Delta t}{\bar{h}_i} |A_{i+1/2}| \right) \frac{\Delta_+ \mathbf{E}_i}{s_{i+1}}, \\ \bar{D}_{x,i-1/2}^\pm &= \bar{h}_i \alpha_i \left( I - \frac{\Delta t}{\alpha_i} |A_{i-1/2}| \right) \left( I - \frac{\Delta t}{\bar{h}_i} |A_{i-1/2}| \right) \Delta_\mp \frac{\Delta_- \mathbf{E}_i}{s_i}, \\ \bar{D}_{x,i+1/2}^\pm &= \bar{h}_i \alpha_i \left( I - \frac{\Delta t}{\alpha_i} |A_{i+1/2}| \right) \left( I - \frac{\Delta t}{\bar{h}_i} |A_{i+1/2}| \right) \Delta_\mp \frac{\Delta_+ \mathbf{E}_i}{s_{i+1}}, \\ \hat{D}_{x,i-1/2}^\pm &= \bar{h}_i \bar{h}_{i\mp 1} \left( \frac{\Delta t}{\bar{h}_{i\mp 1}} |A_{i-1/2}| - I \right) \left( \frac{\Delta t}{\bar{h}_i} |A_{i-1/2}| + I \right) \Delta_\mp \frac{\Delta_- \mathbf{E}_i}{s_i}, \\ \hat{D}_{x,i+1/2}^\pm &= \bar{h}_i \bar{h}_{i\mp 1} \left( \frac{\Delta t}{\bar{h}_{i\mp 1}} |A_{i+1/2}| - I \right) \left( \frac{\Delta t}{\bar{h}_i} |A_{i+1/2}| + I \right) \Delta_\mp \frac{\Delta_+ \mathbf{E}_i}{s_{i+1}}\end{aligned}$$

Here,  $\Delta_\pm \mathbf{U}_i = \pm (\mathbf{U}_{i\pm 1} - \mathbf{U}_i)$ ,  $A^\pm = R \Lambda^\pm R^{-1} = R \left( \frac{A \pm |A|}{2} \right) R^{-1}$ .  $A = \partial \mathbf{E} / \partial \mathbf{U}$  is the Jacobi matrix.  $I$  is the identity matrix.  $R$  and  $R^{-1}$  are the left and right eigenvectors,  $\Lambda$  is the matrix of eigenvalues.  $\alpha_i = s_i$  for  $A^+$  and  $\alpha_i = s_{i+1}$  for  $A^-$ ,  $s_i = \bar{h}_i + \bar{h}_{i-1}$ ,  $d_i = 1/(\bar{h}_i + \bar{h}_{i-1} + \bar{h}_{i-2})$ ,  $\bar{h}_i = (h_i + h_{i-1})/2$ ,  $h_i = x_{i+1} - x_i$ .

In (3), the limiter functions  $\text{limiter1}(a,b)$  and  $\text{limiter2}(a,b)$  are associated with terms of the second and third order of the accuracy, respectively. As limiters, functions  $m(a,b)$ ,  $\text{minmod}(a,b)$  or  $\text{superbee}(a,b)$  are chosen, where

$$\begin{aligned}\text{limiter1}(a,b) &= \text{minmod}(a,b) = \begin{cases} s \cdot \min(|a|, |b|), & \text{if } \text{sign}(a) = \text{sign}(b) = s \\ 0, & \text{else} \end{cases} \\ \text{limiter1}(a,b) &= \text{superbee}(a,b) = \begin{cases} \text{minmod}(2a,b), & \text{if } |a| \leq |b| \\ \text{minmod}(a,2b), & \text{if } |a| > |b| \end{cases} \\ \text{limiter2}(a,b) &= \hat{m}(a,b) = \begin{cases} 1/2 a, & \text{if } |a| \leq |b| \\ 1/2 b, & \text{if } |a| > |b| \end{cases}\end{aligned}\tag{4}$$

The expressions for the fluxes  $\mathbf{F}^m$  and  $\mathbf{G}^m$  are written similarly to  $\mathbf{E}^m$ .

### 3 Results

The numerical computations of the problem are made on the staggered spatial grid with the number of cells  $241 \times 201 \times 201$ , and the time step is  $\Delta t = 0.01$ . The computational domain is  $H_x = 20$ ,  $H_y = 15$  and  $H_z = 10$  calibers. The injector is located in the center of the bottom. The initial parameters of the main flow and the jet are:  $Pr = 0.9$ ,  $M_0 = 1$ ,  $M_\infty = 4$ ,  $T_0 = 800K$ ,  $T_\infty = 1000K$ ,  $Re = 10^4$ , the pressure ratio  $n = 11.72$ .

Since the study focuses on the application of the scheme to the non-uniform grid, the comparison of the computation on the uniform grid with the use of the coordinate system transformation and on the non-uniform grid was preliminarily done in [13]. It was obtained that the behaviour of the flowfield on the non-uniform grid agrees with that on the uniform grid.

As the limiter functions are used in the ENO scheme and there are many different forms of the limiters in the literature [6], for the numerical solution of the (1) the following two kind of the limiters from (4) are selected to investigate its influence on the physics:

$$\text{limiter1}(a, b) = \text{minmod}(a, b), \text{limiter2}(a, b) = \dot{m}(a, b); \quad (5)$$

$$\text{limiter1}(a, b) = 1.1\text{superbee}(a, b), \text{limiter2}(a, b) = \dot{m}(a, b). \quad (6)$$

The choice of these functions is determined by the test performed on the uniform grid by the authors in [14], where the transfer of the hydrogen cube problem was solved to choose the optimal limiter. It was shown there that the use of (1) considerably spreads the original solution while the slight change of the second order limiter (6) gives the significant reduce of the dissipative effects.

The numerical calculations of (1) with the different limiter functions (1), (6) on the non-uniform grid confirm the known dynamics of the transverse sonic jet injection into the supersonic cross-flow, including the shock wave and vortical structures [1,2]. On Fig. 2, the isobars (Fig. 2a,b) and the local Mach number isolines in the supersonic region ( $M > 2$ ) (Fig. 2c,d) are represented in the symmetry section  $xz$  as this plane best demonstrates the distinction between the solutions. The results for the limiters (1) are shown on the left and the results for the limiters (6) are shown on the right. The choice of the limiters has almost no effect on the distribution of the isobars, but more noticeable effect of that on the Mach number distribution can be seen in the supersonic region ( $M > 2$ ).

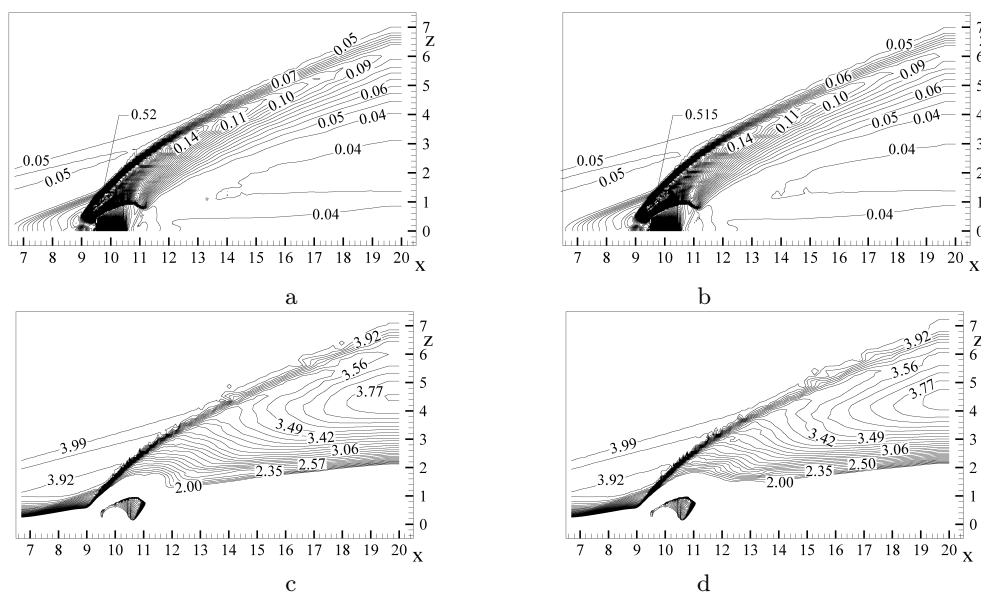


**Fig. 2.** Distribution of the pressure (a,b) and the local Mach number in the supersonic region ( $M > 2$ ) (c, d) in the symmetry section  $xz$  for the limiters (1) (a, c) and for the limiters (6) (b, d),  $n = 11.72$

Despite the slight difference in the dynamic parameters for the limiters (1) and (6), the isolines of the mass fraction clearly show this discrepancy. The distribution of the hydrogen mass fraction in the symmetry section  $xz$  is shown on Fig. 3. Here, the results obtained with the limiters (1) are shown on the left (Fig. 3a), and the results for the limiters (6) are represented on the right (Fig. 3b). It is visible that using limiters (1) considerably increases the upper mixing layer in comparison with the other limiter functions (6). Thus, the maximum value of the height for the

0.3% hydrogen concentration is  $z_{max} = 4.94$  for the (1) and  $z_{max} = 4.902$  for the (6). However, it should be noted that the use of the limiters (6) results in the slight spread of the solution in the region behind the jet.

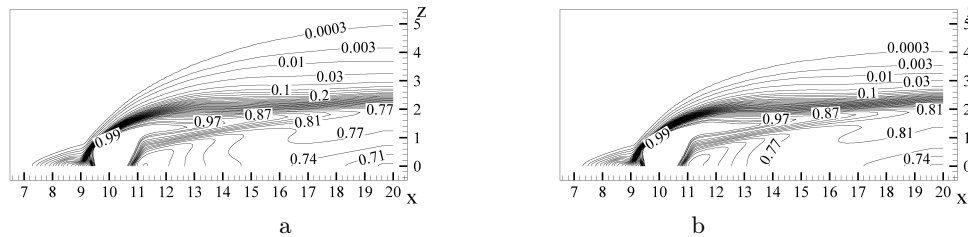


**Fig. 3.** Distribution of the hydrogen mass fraction in the symmetry section  $xz$  for the limiters (1) (a) and for the limiters (6) (b),  $n = 11.72$

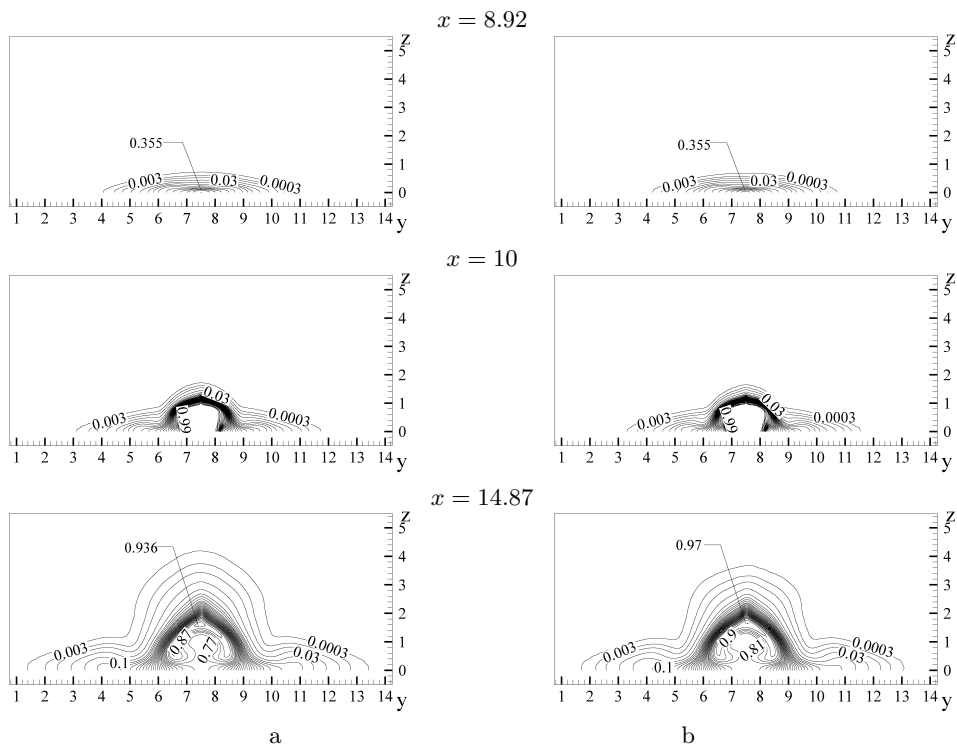
Figure 4 shows the distribution of the hydrogen mass fraction in the different sections  $yz$  for the limiters (1) (on the left, Fig. 4a) and for the limiters (6) (on the right, Fig. 4b). According to the comparison of Figs. 3 and 4, the jet expansion in the  $xz$  section is considerably less than that in the  $yz$  sections. Obviously, it occurs because of the great drift of the injected substance by the main flow.

Figure 4 at the  $x = 8.92$  shows that the hydrogen penetration in the region in front of the jet spreads insignificantly near the wall, i.e. in the subsonic region. The noticeable lateral jet expansion in the injector center (Fig. 4,  $x = 10$ ) is explained by the presence of the lateral vortices which lead to the mainflow velocity reduce. Behind the jet, the accumulation of the injected substance occurs (Fig. 4,  $x = 14.87$ ), then it decreases downstream. In the transverse sections, the significant solution spreading is also can be seen for (1) in comparison with the results for (6).

The effect of the dynamic pressure ratio  $q = (\rho V)_0 / (\rho V)_\infty$  on the jet penetration is shown on the Fig. 5. Numerical experiments were done with parameters of the experiment [15]:  $4 < q < 16$  that corresponds to  $7 < n < 24$ ,  $Re = 9.47 \cdot 10^4$  for  $n = 7.81$  and  $n = 11.72$ ,  $Re = 6.31 \cdot 10^4$  for  $n = 15.61$  and  $n = 23.356$ . The upper curves mark the hydrogen penetration ( $Y_1 = 0.0003$ ), and the lower curves are for the maximum values of the mass fraction of  $H_2$ . Figure 5 shows the noticeable spread of the solution obtained with the limiters (1).

## 4 Summary

In the present paper the third order finite-difference shock-capturing essentially non-oscillatory (ENO) scheme for a non-uniform grid has been developed. Main advantage of the algorithm is that the modification of it from uniform to non-uniform mesh can be done by simple way. The steps of the ENO scheme correspond to the method on the uniform grid written in [12]. The methodology developed here is applied to the numerical simulation of the three-dimensional turbulent steady flowfield generated by the transverse hydrogen injection into the supersonic air cross-flow by solving the RANS equations closed by the  $k - \omega$  turbulent model. The different slope limiters were revised and adapted on the non-uniform meshes. The analysis of the different variations of the limiter functions has been done for the non-uniform ENO scheme. The effect of the limiters on the mixing layer was studied numerically. It was obtained that the unsuccessful choice of some limiters can result in the overgrowth of the mixing layer. The results of the numerical computations show good agreement with the experimental data.



**Fig. 4.** Distribution of the hydrogen mass fraction in the different sections  $yz$  for the limiters (1) (a) and for the limiters (6) (b),  $n = 11.72$

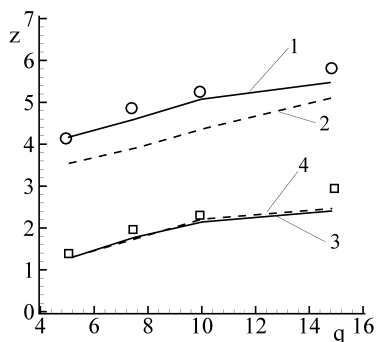


**Fig. 5.** Effect of the dynamic pressure ratio  $q$  on the jet penetration at  $x = 17$ : curve 1 -  $Y_1 = 0.0003$  for the limiters (1); curve 2 -  $Y_1 = 0.0003$  for the limiters (6); curve 3 - maximum value of  $Y_1$  for the limiters (1) ( $Y_1 = 0.541$  for  $n = 7.81$ ,  $Y_1 = 0.693$  for  $n = 11.72$ ,  $Y_1 = 0.817$  for  $n = 15.61$ ,  $Y_1 = 0.93$  for  $n = 23.356$ ); curve 4 - maximum value of  $Y_1$  for the limiters (6) ( $Y_1 = 0.297$  for  $n = 7.81$ ,  $Y_1 = 0.382$  for  $n = 11.72$ ,  $Y_1 = 0.476$  for  $n = 15.61$ ,  $Y_1 = 0.61$  for  $n = 23.356$ );  $\circ$ ,  $\square$  - experiment [15]

## References

1. Gruber, M.R., Nejad, A.S., Chen, T.H., Dutton, J.C.: Transverse Injection from Circular and Elliptic Nozzles into a Supersonic Crossflow. *J. Propulsion and Power*. 16 (3), 449–457 (2000)
2. Ben-Yakar, A., Mungal, M. G., Hanson, R. K.: Time evolution and mixing characteristics of hydrogen and ethylene transverse jets in supersonic crossflows. *Physics of Fluids*, 18, 026101 (2006)
3. Adams, N.A., Shariff, K.: A High-Resolution Hybrid Compact-ENO Scheme for Shock-Turbulence Interaction Problems. *J. Comp. Phys.* 127 (1), 27–51 (1996)
4. Sun, D., Hu, Ch., Cai, T.: Computation of Supersonic Turbulent Flowfield with Transverse Injection. *App. Math. Mech. English Edition*. 23 (1), 107–113 (2002)
5. Amano, R.S., Sun, D.: Numerical Simulation of Supersonic Flowfield with Secondary Injection. In: 24th Congress of ICAS, Yokohama (2004)
6. Berger, M.J., Aftosmis, M.J., Murman, S.E.: Analysis of slope limiters on irregular grids. In: 43rd AIAA Aerospace Sciences Meeting, 2005-0490, Reno, NV (2005)
7. Zeng, X.: A General Approach to Enhance Slope Limiters on Non-Uniform Rectilinear grids. Submitted to *SIAM J. Sci. Comput.* (2014)
8. Bruel, P., Naimanova, A.: Computation of the normal injection of a hydrogen jet into a supersonic air flow. *Thermophysics and Aeromechanics*, 17 (4), 531–542 (2010)
9. Kee, R.J., Rupley, F.M., Miller, J.A.: CHEMKIN-II: a Fortran chemical kinetic package for the analysis of gas-phase chemical kinetics. SANDIA Report SAND89-8009 (1989)
10. Rumsey, C L.: Compressibility considerations for  $k - \omega$  turbulence models in hypersonic boundary layer applications. NASA/TM-2009-215705 (2009)
11. Poinso, T.J., Lele, S.K.: Boundary Conditions for Direct Simulation of Compressible Viscous Flows. *J. Comp. Phys.* 101, 104–129 (1992)
12. Moisseeva, Ye., Naimanova, A.: Supersonic flow of multicomponent gaseous mixture with jet injection. *Computational technologies*, vol. 19, № 5, 51–66 (2014)
13. Moisseeva, Ye., Naimanova, A., Belyayev, Ye., Shakhan, N.: Third order ENO Scheme on Non-uniform Grid for Supersonic Flows. Submitted to *Applied Mechanics and Materials* (2015)
14. Moisseeva, Ye., Naimanova, A.: Numerical simulation of the transverse hydrogen injection into a supersonic turbulent airstream. In: *Proceedings of Advanced Problems of Mechanics (APM) 2014*, pp. 358–365. St.-Petersburg, Russia (2014)
15. Rogers, R. C.: A study of the mixing of hydrogen injected normal to a supersonic airstream. NASA TN D-6114 (1971)